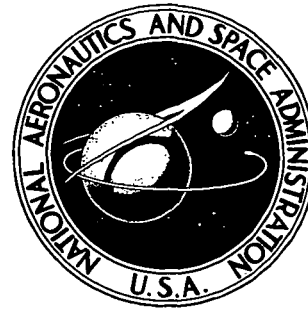


N73-12269

NASA TECHNICAL NOTE



NASA TN D-7076

NASA TN D-7076

**CASE FILE
COPY**

**EFFECTS OF INSTALLATION CAUSED
FLOW DISTORTION ON NOISE
FROM A FAN DESIGNED
FOR TURBOFAN ENGINES**

*by Frederick P. Povinelli, James H. Dittmar,
and Richard P. Woodward*

*Lewis Research Center
Cleveland, Ohio 44135*

1. Report No. NASA TN D-7076	2. Government Accession No.	3. Recipient's Catalog No.	
4. Title and Subtitle EFFECTS OF INSTALLATION CAUSED FLOW DISTORTION ON NOISE FROM A FAN DESIGNED FOR TURBOFAN ENGINES		5. Report Date November 1972	6. Performing Organization Code
		8. Performing Organization Report No. E-7088	10. Work Unit No. 501-24
7. Author(s) Frederick P. Povinelli, James H. Dittmar, and Richard P. Woodward		11. Contract or Grant No.	
		13. Type of Report and Period Covered Technical Note	
9. Performing Organization Name and Address Lewis Research Center National Aeronautics and Space Administration Cleveland, Ohio 44135		14. Sponsoring Agency Code	
		12. Sponsoring Agency Name and Address National Aeronautics and Space Administration Washington, D. C. 20546	
15. Supplementary Notes			
16. Abstract <p>Far-field noise measurements were taken for three different installations of essentially the same fan. The installation with the most uniform inlet flow resulted in fan-blade-passage tone sound pressure levels more than 10 dB lower than the installation with more nonuniform inflow. Perceived noise levels were computed for the various installations and compared. Some measurements of inlet flow distortion were made and used in a blade-passage noise generation theory to predict the effects of distortion on noise. Good agreement was obtained between the prediction and the measured effect. Possible origins of the distortion were identified by observation of tuft action in the vicinity of the inlet.</p>			
17. Key Words (Suggested by Author(s)) Fan noise Flow distortion Noise Turbofan		18. Distribution Statement Unclassified - unlimited	
19. Security Classif. (of this report) Unclassified	20. Security Classif. (of this page) Unclassified	21. No. of Pages 39	22. Price* \$3.00

* For sale by the National Technical Information Service, Springfield, Virginia 22151

EFFECTS OF INSTALLATION CAUSED FLOW DISTORTION ON NOISE FROM

A FAN DESIGNED FOR TURBOFAN ENGINES

by Frederick P. Povinelli, James H. Dittmar, and Richard P. Woodward

Lewis Research Center

SUMMARY

Three installations of essentially an identical fan were used to obtain fan noise data. In two of the installations the fan was driven by a shaft in the inlet; in the other installation the fan was driven from the rear. These various installations and the structures associated with them were assumed to result in different amounts of inlet flow distortion. The rear-drive installation had the least amount of inlet flow distortion.

Differences in fan-blade-passage tone sound pressure level of more than 10 dB were measured between the rear-drive and front-drive versions, with the rear-drive installation producing less blade-passage noise. Differences in blade-passage tone were greatest in the front quadrant and at higher fan speeds. Despite the lower blade-passage tones, the rear-drive installation was unacceptable because of the additional broadband noise generated by the exhaust flow over the shaft and supporting structures.

One-third octave spectra for the front-drive installations were corrected to have discrete tones of the magnitude measured for the rear-drive installation. Perceived noise levels were calculated from both the corrected and measured spectra and compared. The fans had their highest noise levels in the aft quadrant, and the maximum discrete tone corrections were in the front quadrant. Thus maximum sideline perceived noise levels were reduced only 2.1 PNdB or less when corrected for discrete tones. In general, the perceived noise levels were lower and were affected more by the correction at takeoff speed than at approach speed. The effect of correcting for discrete tones was also calculated for level flyover effective perceived noise levels (EPNL). The correction resulted in a maximum reduction of 4.4 EPNdB.

Some measurements of inlet flow distortion were made and used in a blade-passage noise generation theory to predict the effects of distortion on noise. Good agreement was obtained between the predicted and measured noise differences in the front-drive and rear-drive installations. Possible origins of the inlet flow distortion were identified by observations of tuft action in the vicinity of the inlet.

INTRODUCTION

As part of a program to develop a quiet engine for conventional takeoff and landing (CTOL) aircraft, full-scale fans for use on large-bypass-ratio turbofan engines are being tested in an outdoor noise rig at the Lewis Research Center (refs. 1 to 3). Fans designed to produce low noise levels are evaluated based on far-field noise measurements, and the best candidates selected for incorporation into full-scale turbofan engine testing. Full-scale fans for short takeoff and landing (STOL) aircraft are also being tested in this fan test rig.

The noise measured at the blade-passage frequency from the first CTOL fan tested in the rig (refs. 1 and 2) was greater than anticipated and was attributed to a measured nonuniform inlet airflow presumably caused by a concrete support structure upstream of the inlet. The distorted inflow is related to the noise output of the fan using the theory of Morse and Ingard (ref. 4). The theory indicates that even small amounts of flow inhomogeneities can have significant effects on the sound radiated from a propeller.

In this report the far-field noise data from three different installations of essentially the same fan are examined. In the first installation the fan was installed as in reference 1. In an attempt to minimize the inlet flow distortion, the fan was also installed in two other ways in the same test stand with presumably different amounts of inlet flow distortion for each installation. The installation effects on overall noise, on fan-blade-passage tone, and on perceived noise levels are determined. Some inlet flow distortion measurements were made for one of the installations. The measured distortion values were used in the theory of reference 4, and the predicted noise levels were compared with measured levels.

APPARATUS AND PROCEDURE

Fan Description

Three fans, very similar in design, have been used in the course of this study. All were suitable for use on aircraft engines in the 89 000-newton (20 000-lbf) thrust class and were nominally 1.8 meters (6 ft) in diameter. Acoustic data were obtained for two 1.5 pressure ratio fans while a 1.4 pressure ratio fan was used for the distortion tests. One of the 1.5 pressure ratio fans, designated as QF-1, has been described in detail in reference 1. Some important features of the QF-1 fan are given here, and the differences between it and the other two fans are mentioned.

1.5 pressure ratio fans. - A cutaway view of QF-1 fan as installed for references 1 to 3 and for one of the installations compared herein is shown in figure 1. The pertinent

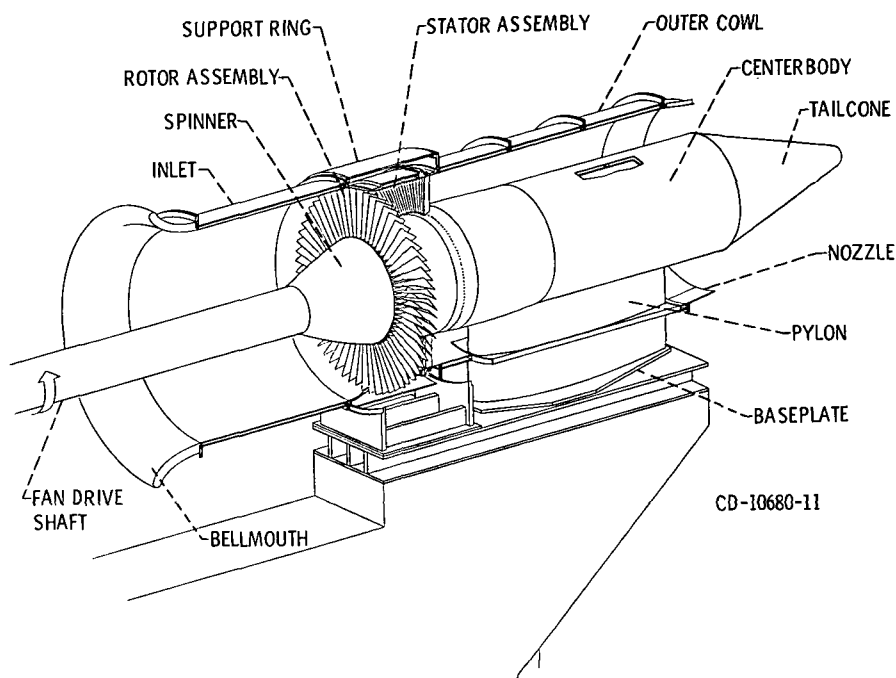


Figure 1. - Front-drive fan nacelle assembly.

design values of this fan are as follows:

Rotor tip diameter, m (in.)	1.824 (71.81)
Stator tip diameter, m (in.)	1.726 (67.94)
Rotor tip speed (cruise design value, corrected), m/sec (ft/sec)	337.4 (1107)
Design stagnation pressure ratio	1.5
Design weight flow (corrected), kg/sec (lbm/sec)	396 (873)
Rotor hub-tip radius ratio (inflow face).	0.50
Stator hub-tip radius ratio	0.59
Rotor-stator spacing (rotor trailing edge to stator leading edge at the hub), cm (in.)	50.8 (20)
Number of rotor blades	53
Number of stator blades	112
Rotor chord length, cm (in.)	13.97 (5.5)
Stator chord length, cm (in.)	6.83 (2.69)

Aerodynamic parameters have been corrected to NACA standard sea-level atmospheric conditions of 288.2 K (518.7° R) and 1.013×10^5 newtons per square meter (2116.2 lbf/ft²).

Another 1.5 pressure ratio fan, designated as QF-2, was used for some of the acoustic tests. It was designed to be an opposite rotation version of QF-1. The only

difference between these two fans was in the stator blade end attachments at the tip. The QF-1 stator blade end attachments are shown in reference 1. A smoother fairing of the blade section to the cylindrical end attachment was used on QF-2 to give better aerodynamic flow at the stator tips. This small difference in the two fans should not result in any significant differences in fan noise generation.

1.4 pressure ratio fan. - A 1.4 pressure ratio fan was used for the distortion tests and designated as QF-3. This fan was designed to be as identical to QF-1 and QF-2 as possible but to generate a 1.4 pressure ratio across the fan stage instead of 1.5. The lower pressure rise was accomplished by designing the rotor and stator blades with less camber. No acoustic data for the 1.4 pressure ratio QF-3 fan are presented in this report.

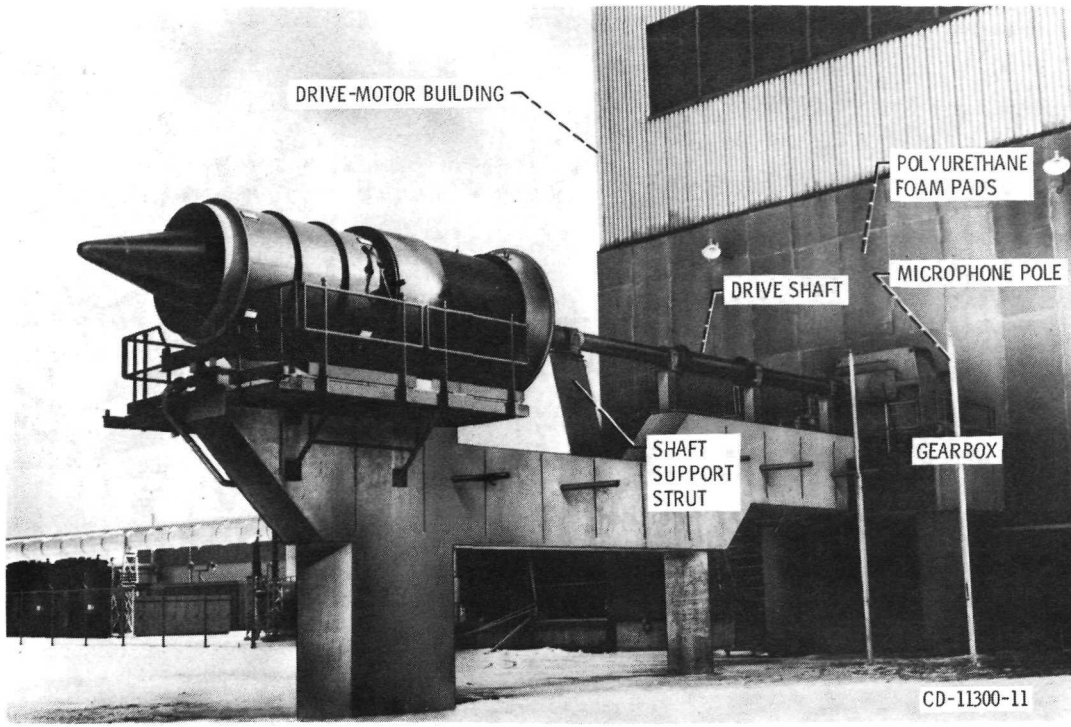
Test Stand Description

The three fans described previously were tested in the quiet fan outdoor test stand at the Lewis Research Center. In the course of this study the test stand was modified twice, and it is the effects of these modifications on the noise generated by the fans which comprise the main portion of this report.

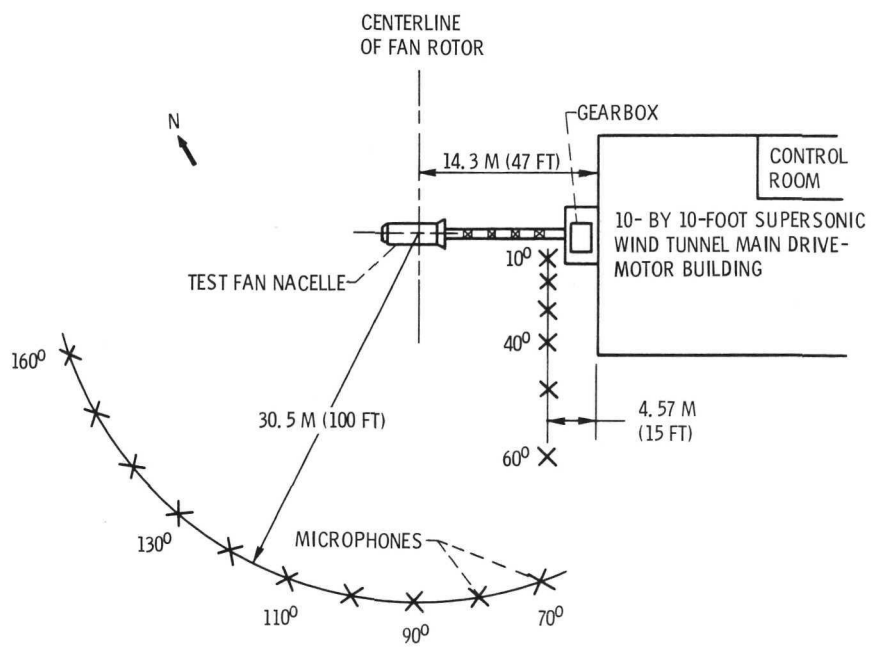
Short-shaft front-drive installation. - The QF-1 fan was tested in the installation as shown in figure 2 and described in detail in references 1 to 3. This setup shall hereinafter be called the short-shaft front-drive installation. The fan was driven by electric motors (inside the building) through a gearbox and through the shaft shown entering the fan nacelle inlet (fig. 2(a)). The shaft rotation was counterclockwise when viewed looking into the inlet. Open-cell polyurethane foam, 15.2 centimeters (6 in.) thick, was mounted on the drivemotor building wall and adequately eliminated reflection effects above 400 hertz (ref. 1).

A one-piece concrete structure, extending underneath the inlet, supported the fan nacelle and shaft. The shaft centerline was 5.8 meters (19 ft) above the asphalt ground plane at the fan rotor position. The swept shaft support strut closest to the fan inlet was made in a streamline airfoil shape to minimize inlet flow distortion. The top of the trailing edge of this strut was approximately 3.35 meters (11 ft) upstream of the fan rotor.

The plan view of the short-shaft front-drive installation (fig. 2(b)) shows the microphone locations and the fan position in relation to the drive-motor building. Microphones were positioned on the poles at the shaft centerline elevation and extended around the fan in 10° spacings from 10° to 160° measured from the fan inlet centerline. Microphones from 70° to 160° were on a 30.5-meter (100-ft) radius from the fan rotor center while those from 10° to 60° were at a fixed 4.57-meter (15-ft) distance from the building wall. The fan rotor plane was 14.3 meters (47 ft) from the building wall.

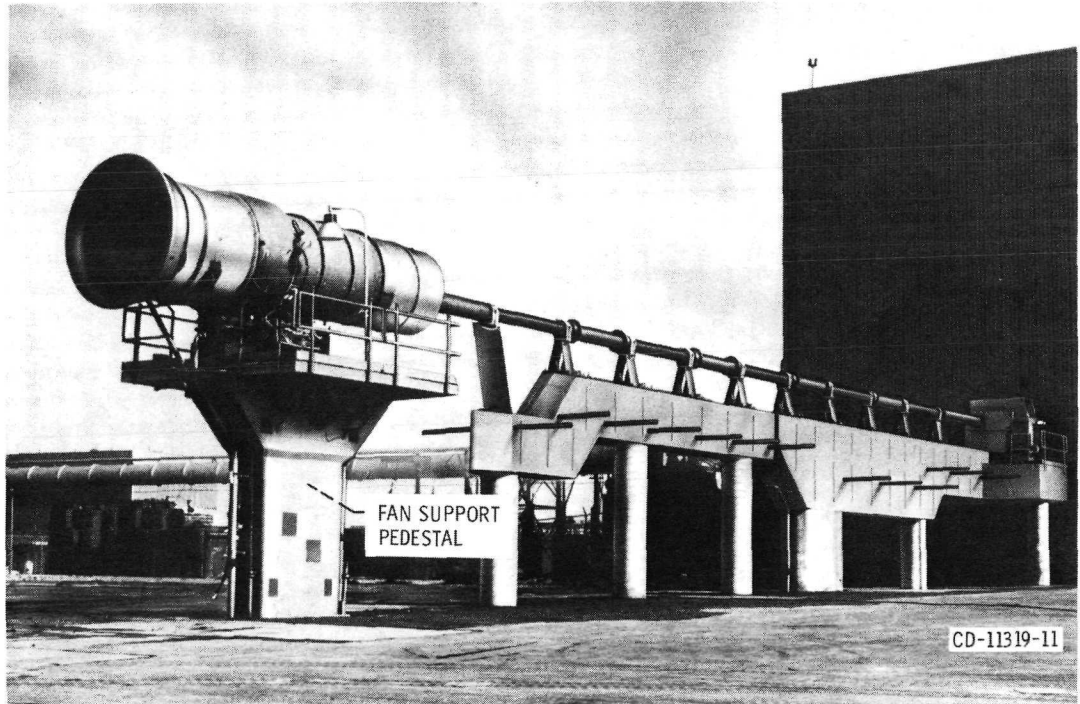


(a) PHOTOGRAPH OF TEST SITE.

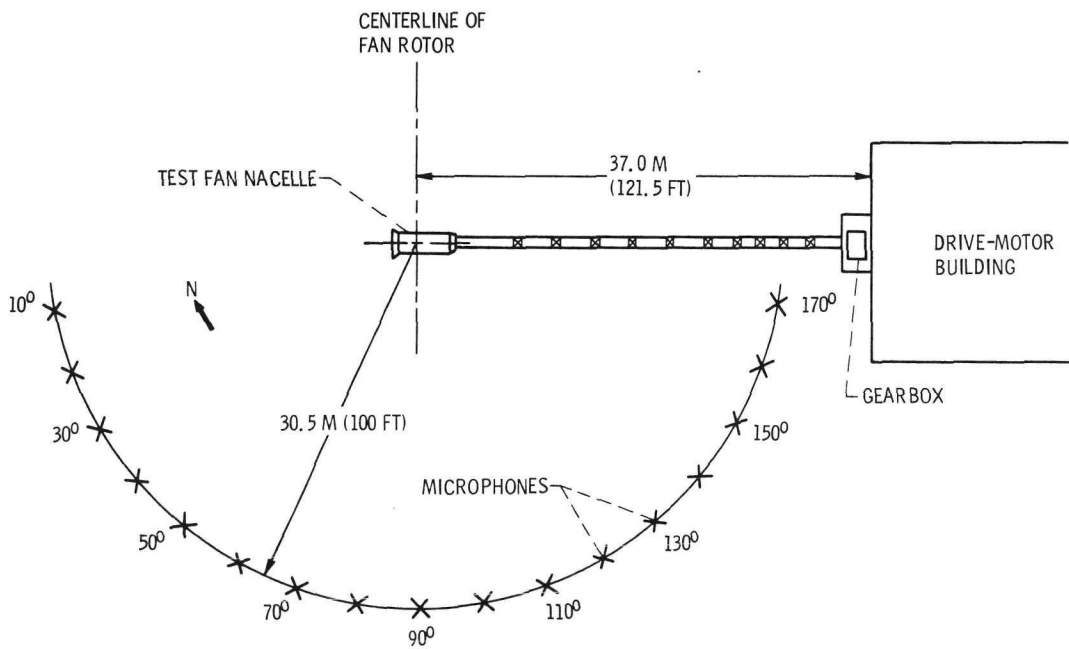


(b) PLAN VIEW OF TEST SITE.

Figure 2. - Short-shaft front-drive installation.

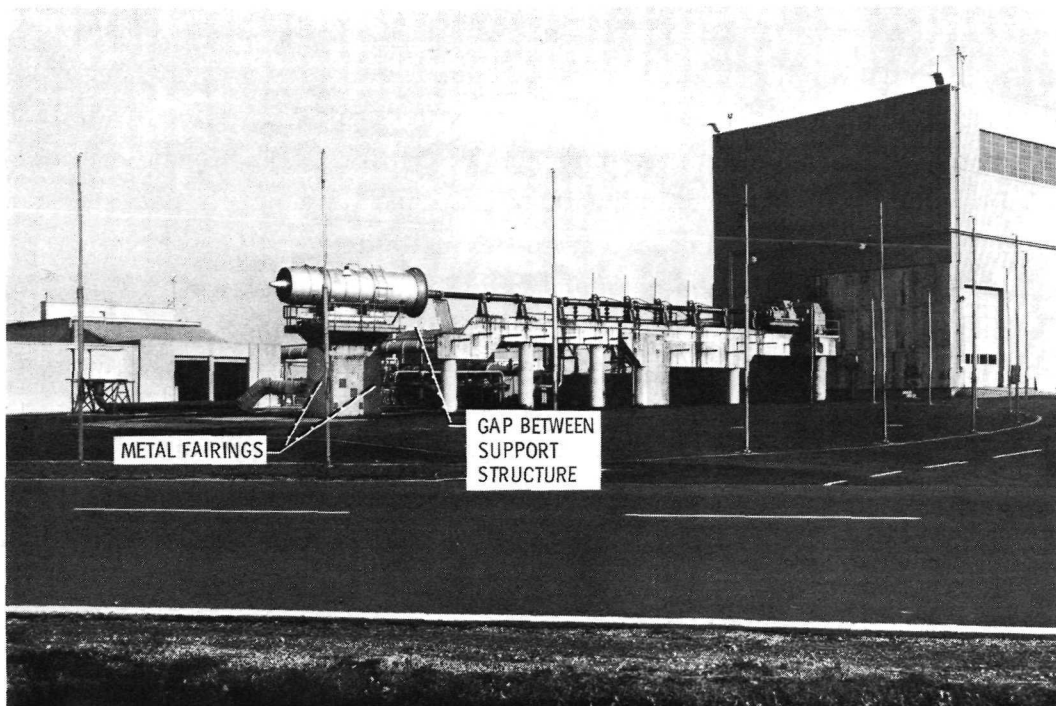


(a) PHOTOGRAPH OF TEST SITE.

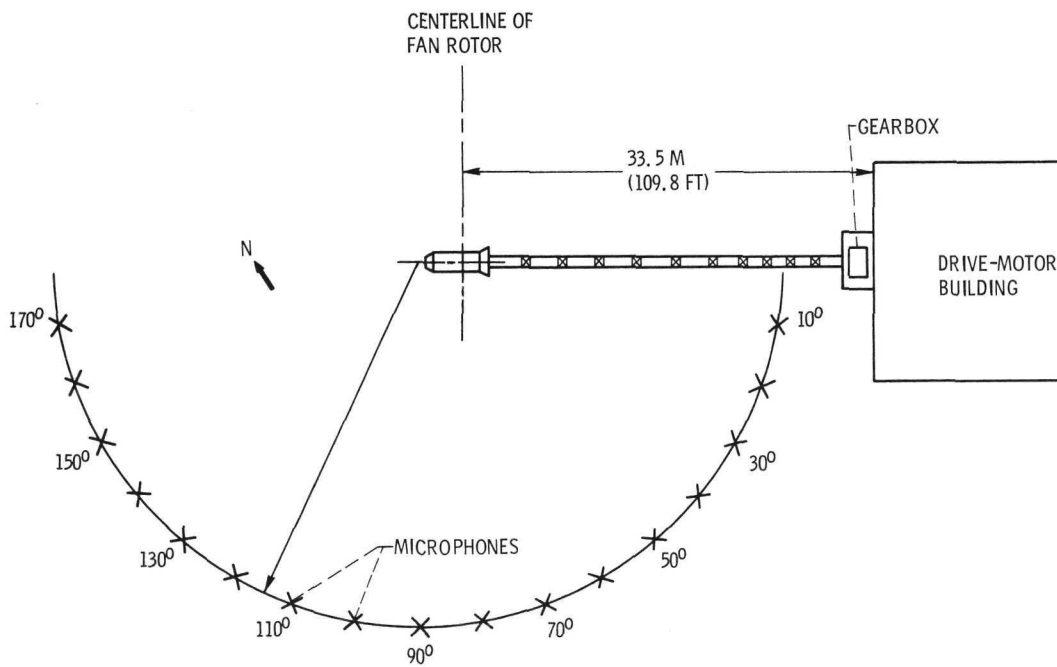


(b) PLAN VIEW OF TEST SITE.

Figure 3. - Long-shaft rear-drive installation.



(a) PHOTOGRAPH OF TEST SITE.



(b) PLAN VIEW OF TEST SITE.

Figure 4. - Long-shaft front-drive installation.

Long-shaft rear-drive installation. - The QF-2 fan was first tested in the installation shown in figure 3. The drive shaft was lengthened and connected to the fan through the exhaust end of the nacelle rather than through the inlet (fig. 3(a)), thus the name of long-shaft rear-drive for this installation. The shaft elevation was unchanged resulting in slightly greater than 5.8-meter (19-ft) height of the shaft centerline at the fan rotor due to the ground slope away from the drive-motor building. The lengthened shaft was supported by extending the concrete structure. A separate concrete pedestal was erected to support the fan nacelle. Also before taking acoustic data, polyurethane foam pads were mounted on the wall as in the previous installation. The plan view (fig. 3(b)) of the test site shows the fan rotor now 37 meters (121.5 ft) from the building and the microphone poles repositioned so that all microphones were on a 30.5-meter (100-ft) radius from the fan rotor center and at the rotor axis elevation.

Long-shaft front-drive installation. - The QF-2 fan was also tested in the installation shown in figure 4. The identical fan nacelle as used in the long-shaft rear-drive installation was rotated 180° and the fan was now driven through the inlet. The gearbox was used to reverse the direction of shaft rotation. The separation between the concrete structures is clearly visible in figure 4(a). This gap of 3.05 meters (10 ft) between the two support pedestals eliminated the concrete structure immediately underneath the inlet which was present in the short-shaft installation. Metal fairings have been added to both ends of the fan support pedestal to reduce the possibility of inlet flow distortions caused by nonuniform flow being pulled into the inlet from downstream.

The plan view of this third installation is given in figure 4(b). The rotor face was 33.5 meters (109.8 ft) from the building and the microphone locations have not been changed from the rear-drive installation. Thus the center of the microphone arc was no longer in the plane of the rotor but rather in the exhaust flow. The microphones were no longer positioned at equal 10° increments or even 20.5-meter (100-ft) distances relative to the rotor. This has been accounted for in the data comparisons of the three installations. This long-shaft front-drive installation was also used for the 1.4 pressure ratio QF-3 fan reported herein and for all subsequent fans tested in the NASA quiet fan development program to date.

Acoustic Instrumentation and Data Reduction

A complete description of the acoustic instrumentation and the data acquisition techniques is given in reference 1. Some aspects of the acoustic data system are given here for convenience.

Omnidirectional condenser microphones 1.3 centimeters (0.5 in.) in diameter were used to pick up the noise signal generated by the fan. At each test condition three

sets of data were taken to minimize short-term fluctuations in fan or background noise. Each microphone signal was fed through approximately 150 meters (500 ft) of cable to the control room where the signal was conditioned and recorded on a 14-channel FM magnetic tape recorder. The dropoff in frequency response due to the long cable length discussed in reference 1 was overcome for the long-shaft installations by increasing the power to drive the cathode follower preamplifiers.

Acoustic data from all three installations were resolved into one-third octaves from 50 to 20 000 hertz. An improved analyzer over that used in reference 1 was employed. A 4-second average of sound pressure level was obtained for each one-third octave filter and stored on magnetic tape for use in digital computer program calculations. The sound pressure levels for the three samples for each test condition were averaged and were corrected to a 30.5-meter (100-ft) radius for those microphones which were not at this distance, using the inverse squared distance rule. These corrections were applied to the data obtained at 10° to 60° for the short-shaft installation and to all data obtained for the long-shaft front-drive installation. The data were also corrected to standard-day conditions (70 percent relative humidity; 288.2 K, 59° F) using the methods of reference 5 and for cable losses for the short-shaft installation. No corrections were made for ground reflection effects.

Data tapes were also reduced on a 32-hertz constant bandwidth analyzer from 0 to 10 000 hertz to allow finer resolution of the noise spectra. At least three narrow-band spectra were obtained for each angle at each test condition. The sound pressure levels used from these narrow bands were average values of the spectral readings.

Distortion Tests

In order to better define the origin, extent, and magnitude of the flow distortion in a front-drive installation, some tests were made using the QF-3 fan (1.4 pressure ratio) in the long-shaft front-drive installation. A rake with closely spaced total pressure tubes was used to determine pressures in the inlet, and tufts were used in the vicinity of the inlet to visualize the flow direction and uniformity.

Total pressure rake. - An 88-tube total pressure rake (fig. 5) was used to determine velocity defect in the QF-3 inlet. Tubes were spaced on 1.27-centimeter (0.5-in.) centers which allowed coverage of an area approximately 10.2 by 15.2 centimeters (4 by 6 in.). The rake was designed based on the total pressure measurements obtained on QF-1 in the short-shaft installation (refs. 1 and 2). The rake was installed through the outer casing of the inlet at the 6 o'clock location. The survey plane was approximately 0.3 meter (1 ft) upstream of the fan rotor. The pressure tubes were connected with flexible tubing to a 96-tube manometer board located on the ground next

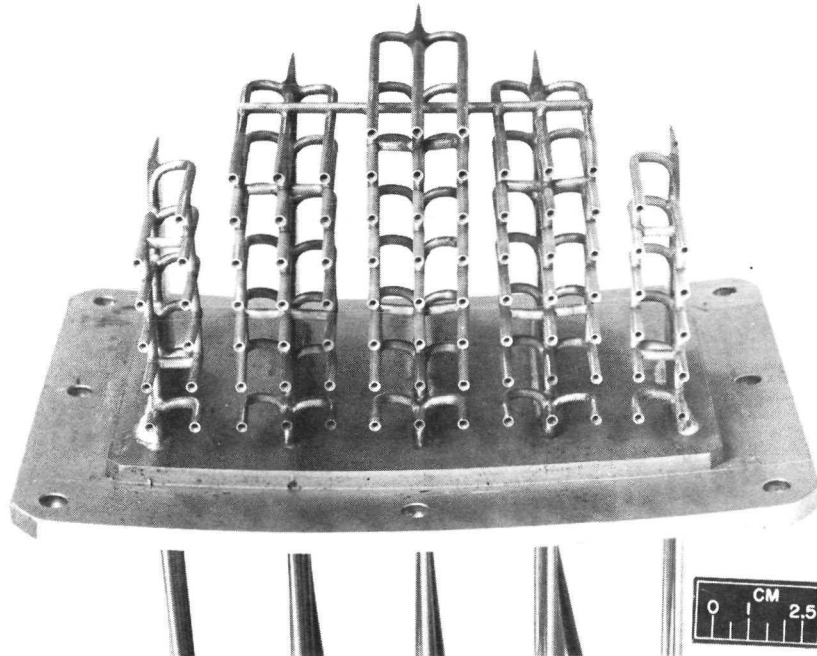


Figure 5. - Total pressure tube rake used for inlet flow distortion measurements.




to the fan support pedestal. Pressure readings were obtained by photographing the manometer board with a motion picture camera.

Tufts. - Yarn tufts approximately 7.6 centimeters (3 in.) in length were positioned near the fan inlet to visually determine flow direction and regions of disturbed flow. The tufts were located on the streamlined strut, on eight horizontal wires strung underneath the bellmouth, on vertical wires mounted beneath and downstream of the bellmouth, and around the outer casing at the bellmouth-inlet flange. Tuft action was recorded with a motion picture camera.

Test Conditions

Although a range of fan speeds was obtained in the course of the testing, only two test speeds have been selected for presentation here. A list of acoustic test conditions is given in table I. Corrected fan speeds were used which corresponded to 60 percent and 90 percent of standard-day cruise design speed. At 60 percent of design speed, aircraft approach power settings were simulated and 90 percent of design speed takeoff conditions were simulated. Since corrected fan speeds were set at each condition, the mechanical speed of the fan for the various installations differed. This resulted in the blade-passage tone frequency variations as noted in table I. Data were obtained only when the wind velocity was 18.5 kilometers per hour (10 knots) or less. Exhaust nozzle

TABLE I. - ACOUSTIC TEST CONDITIONS

Installation	Fan	Temperature		Relative humidity, percent	Wind velocity		Wind direction	Percent of design nozzle area	Percent of design speed (sea-level corrected)	Mechanical rotor speed, rpm	Blade-passage tone frequency, Hz
		K	°F		km/hr	knots					
Short-shaft front-drive 	QF-1	271	28	72	11.1 to 18.5	6 to 10	NNE	97	60	2057	1817
									90	3084	2724
Long-shaft rear-drive 	QF-2	270	26	78	5.6 to 11.1	3 to 6	N	97	60	2045	1806
									90	3064	2708
Long-shaft front-drive 	QF-2	286	55	78	9.3	5	SSE	100	60	2112	1866
									90	3167	2798

area was set at 100 percent of design nozzle area for the long-shaft front-drive installation and at 97 percent of design area for the other two installations. The nozzle was redesigned for the long-shaft front-drive installation and resulted in a change in the nozzle contraction and in the exposed length of tailcone (compare figs. 2 and 4). This may have had a slight effect on the noise levels measured at the far aft angles as will be shown.

The three installation symbols shown in the left-hand column of table I will be used in future figures to identify the various installations.

RESULTS AND DISCUSSION

Since the quiet fan test rig is used to evaluate the acoustic performance of component fans, inlet flow distortion instrumentation is not installed as a matter of practice. Thus distortion measurements were not made for each installation considered herein. It is reasonable to assume, however, that different amounts of inlet flow distortion existed for each installation even though no comparative inlet pressure measurements are available. The rear-drive installation presented no obstructions upstream of the inlet and should therefore have the least inlet flow distortion of the configurations tested. Of the two front-drive installations, the long-shaft version with the separation in the concrete support structures and with the fairings on the fan nacelle support pedestal should provide some improvement over the short-shaft version.

As noted earlier, some distortion measurements were made for a 1.4 pressure ratio fan installed in the long-shaft front-drive configuration. For this installation the distortion was characterized well enough to allow a calculation to be made to predict the effects of this distortion on the fan noise. The distortion results will be discussed after noise data comparisons are made for the three installations.

Noise Results

Overall sound pressure level. - Comparison of the overall sound pressure levels (OASPL) for the three installations as a function of the angular position from the inlet are shown in figure 6. All data have been corrected to standard-day conditions at a 30.5-meter (100-ft) radius. OASPL's allow gross comparisons of the noise levels of the three installations. Comparison of the two front-drive installations show about the same overall levels for both speeds except at angles greater than about 130° and at two angles in the front quadrant at nominally 20° and 50° . Since the front quadrant directivity patterns at both 60 and 90 percent speed for the front-drive long-shaft installation were uncharacteristic of directivities measured for other fans run in this test stand, it

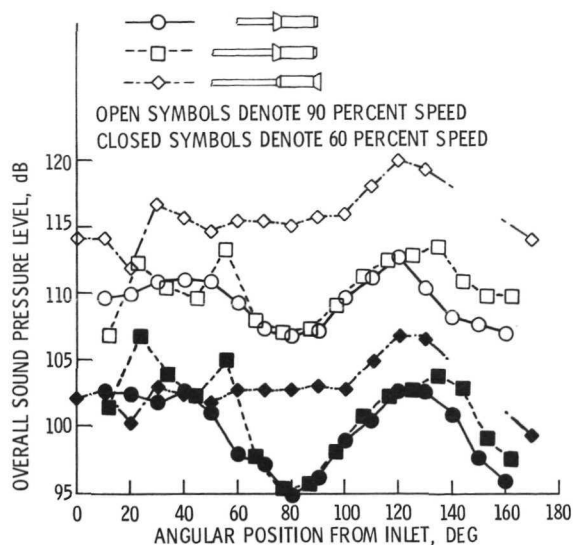


Figure 6. - Angular distribution of overall sound pressure level on 30.5-meter (100-ft) radius for three fan installations. (Standard-day conditions.)

was concluded that a calibration error probably existed for the nominal 20° and 50° microphone measurements. These errors do not significantly affect the results and therefore the data are reported as measured. Aft of 130° the differences in OASPL between the two front-drive installations was possibly due to the redesigned exhaust nozzle.

The significant features to note in figure 6 are the generally higher OASPL values for the rear-drive installation in comparison to the two front-drive versions. As will be shown in narrow-band spectra, low frequency noise controlled the OASPL values for the rear-drive installation especially for the aft quadrant angles. This was due to the high velocity fan exhaust flow impinging and scrubbing on the drive shaft, its supports, and the concrete structure and on the turning of the flow by the building wall. In addition, the force of the exhaust flow caused dangerously high deflections of the corrugated sheet metal building wall. Thus for both acoustic and structural reasons the rear-drive installation was unacceptable.

Narrow-band spectra. - Even though there was significant low frequency content to the noise of the rear-drive installation, narrow-band analyses of the data reveal some interesting features of this cleaner inlet installation. Comparisons of narrow-band spectra for the three installations at 90 percent speed are given in figure 7. Figure 7(a) is for a nominal angular position of 50° , approximately where the front quadrant noise peaked, and figure 7(b) is for the approximate aft quadrant noise peak at 120° . The large peaks in the spectra at 2700 to 2800 hertz correspond to the blade-passage frequency and the smaller peaks represent harmonics of this fundamental frequency. In the front quadrant (fig. 7(a)) sound pressure levels (SPL) at the blade-passage frequency

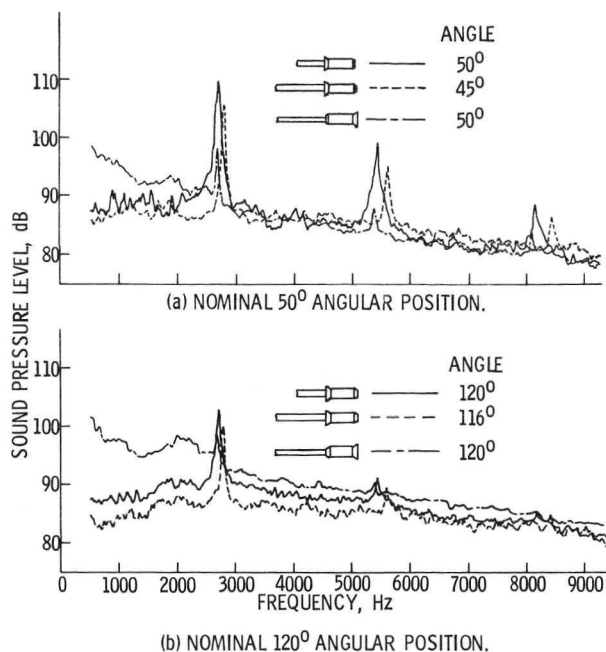


Figure 7. - Narrow-band (32-Hz bandwidth) sound pressure level spectra on 30.5-meter (100-ft) radius; 90 percent speed.

and its harmonics for the rear-drive installation were substantially below the two front-drive cases. This is attributed to the lack of structures upstream of the inlet and presumably less inlet flow distortion in the rear-drive case.

Of the two front-drive installations the long-shaft version had somewhat lower discrete tone content than did the short-shaft version. This may be due to the difference in distortion generated by flow over the different concrete structures in the vicinity of the inlet. The variations in frequency of the discrete tones were because of differences in mechanical fan speed. The higher low frequency noise for the rear-drive case is evident below about 2100 hertz. Over the rest of the spectrum the broadband noise of the three installations was comparable.

For the rear quadrant noise shown in figure 7(b), the broadband noise for the rear-drive installation increased above that for the two front-drive cases over the entire spectrum. The increase was due to the proximity of the 120° microphone to the additional noise source caused by the exhaust flow over the structures. The spike caused by the blade-passage tone for the rear-drive case was still less than that for the two front-drive cases even in the aft quadrant.

Since the effects of the type of inlet flow distortion present in this rig are manifested most dramatically in the discrete tones generated by a fan, the blade-passage tone content was determined for each installation as a function of angular position. SPL values for blade-passage tone were determined from the narrow-band spectra (fig. 7). Broadband

SPL's were faired in below the spikes in the spectra. The broadband SPL's were subtracted from the measured SPL's of the spikes to determine the level of the blade-passage tones. For spectra in which the spikes extended 10 dB or more above the broadband levels, the blade-passage tones were within 1/2 dB of the SPL of the spikes. An example of a spectra where the spike did not extend 10 dB above the broadband is shown in figure 7(b) for the rear-drive installation. Here the blade-passage tone was resolved as the SPL of the spike, 99 dB, minus the broadband level, 95 dB. Subtracting on an energy basis resulted in a blade-passage tone of 96.8 dB.

Blade-passage tones determined in this manner are shown in figure 8(a) for 90 percent speed and in figure 8(b) for 60 percent speed for the three installations. All values are the acoustic energy averages from at least three narrow-band spectra. Therefore, the blade-passage tones shown in figure 8(a) may not agree exactly with those measured from figure 7. For 90 percent speed the rear-drive installation with the cleaner inlet had consistently lower blade-passage tone levels than the two front-drive installa-

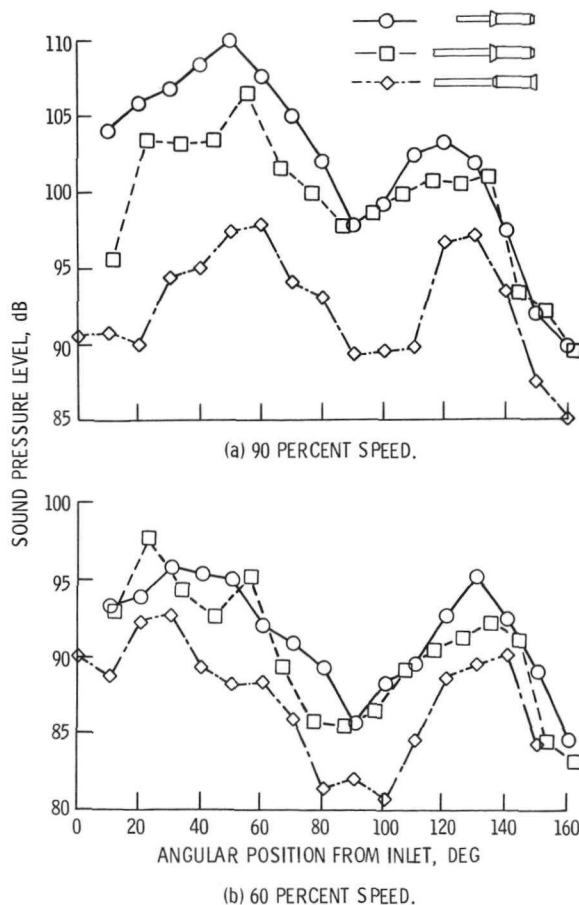


Figure 8. - Angular distribution of blade-passage tone from narrow-band spectra on 30.5-meter (100-ft) radius. (Standard-day conditions.)

tions with higher levels of inlet flow distortion. The largest differences occurred in the forward radiated noise with a maximum difference of at least 10 dB over the front 70° between the rear-drive version and the short-shaft front-drive version. A somewhat lesser blade-passage tone was generated in the front quadrant when the front-drive installation was run with the long shaft as compared to the short shaft. The front-drive installations had approximately 6 dB more front quadrant peak noise than aft quadrant peak noise whereas the rear-drive front and aft quadrant peaks were about the same. At 60 percent speed (fig. 8(b)) the rear-drive installation still had consistently less blade-passage tone content but not nearly as great a difference as at the higher speed. This can be explained by several possible observations. The distortion would be less at the lower inlet velocity, and also the blades would be less sensitive to changes in angle of attack at the lower speed, since they have a larger range of angle of attack over which the drag coefficient is a minimum (i. e., a wider loss bucket).

At present, the Lewis quiet fan test site is in the long-shaft front-drive configuration. Based on the blade-passage data presented in figure 8 it is likely that all fans tested in this configuration would have blade-passage tone levels higher than would be obtained with a more uniform inlet flow. Thus, the blade-passage tones obtained from fans installed in this front-drive configuration would likely be conservative; that is, the same fan installed in an airplane engine would probably generate less blade-passage noise. Since the additional noise generated due to flow distortion is a function of fan design as well as the type of distortion (as will be shown in appendix A), the results shown in figure 8 for the 1.5 pressure ratio fans should not be used to correct other fan noise data obtained in this installation.

The remainder of this noise results section will be concerned with rating techniques for the fans tested here and with the effects of flow distortion on these ratings.

One-third octave spectra. - A commonly used noise data presentation and one from which perceived noise levels are determined is the one-third octave spectrum. Comparisons of the one-third octave spectra for the three installations are shown in figure 9. The same angles as shown for the narrow-band spectra (fig. 7) are presented. For both angular positions (nominal 50° and 120°) the two front-drive installations had very similar SPL's. Due to the additional noise from flow over the shaft and its supports, the rear-drive installation had higher levels than the front-drive cases up to the 2500-hertz band in the front quadrant (fig. 9(a)) and over the entire spectrum in the aft quadrant (fig. 9(b)). At the front quadrant angle it can be seen that the blade-passage tone for the two front-drive installations was split differently between the 2500- and 3150-hertz frequency bands because of the different mechanical speeds.

Discrete tone corrections. - To determine the effect of flow distortion on rating techniques, the one-third octave spectra for the two front-drive installations were corrected so that they had the discrete tone levels which resulted from the cleaner inlet

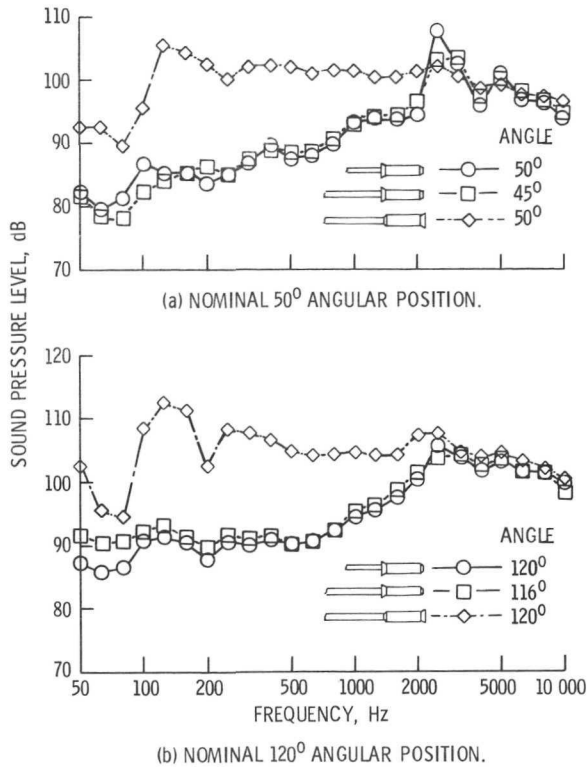


Figure 9. - One-third octave sound pressure level spectra on 30.5-meter (100-ft) radius; 90 percent speed. (Standard-day conditions.)

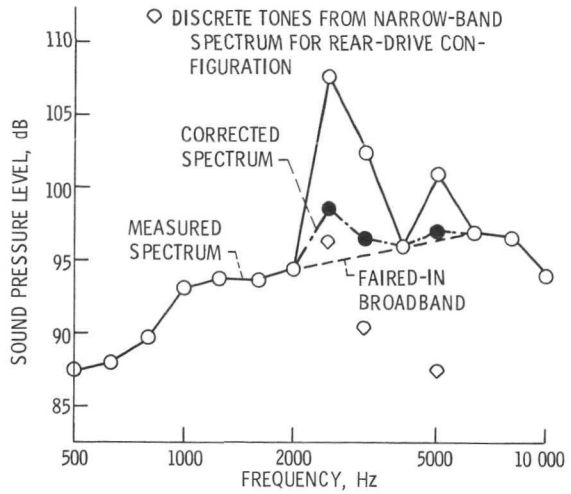


Figure 10. - Method of correcting one-third octave spectra for discrete tones. Short-shaft front-drive configuration; 50° angular position; 90 percent speed.

rear-drive installation. It was reasoned that a uniform flow inlet would have blade-passage tones at least as low as those measured from the rear-drive installation. The method of one-third octave spectrum correction is illustrated in figure 10 for the short-shaft front-drive installation at the 50° angular position and 90 percent speed. Broadband levels for the front-drive installations were faired-in as shown by the dashed lines. Values for the blade-passage tone and its harmonic for the rear-drive installation were determined from narrow-band spectra. These discrete tone values were added to the faired-in broadband level and resulted in the corrected spectrum. Since the fundamental blade-passage tone was split between two one-third octave bands, it was necessary to correspondingly split the rear-drive fundamental tone before addition to the broadband level. The harmonic of the fundamental tone was also split between two one-third octave bands but since the harmonic was almost entirely within the 5000-hertz band and was considerably below the broadband, no corrections were made to the 6300-hertz band.

This type correction was made at all angular positions for both front-drive installations. For the long-shaft case the harmonic was more evenly split into two frequency bands due to the higher mechanical speed. Thus corrections were also made to the 6300-hertz frequency band in this case. Recalling that this long-shaft installation had

measurements made at uneven angular positions, values for the blade-passage tone were read from figure 8 at the appropriate angle by straight line interpolation between the measured points, and similarly for the harmonic tone.

The method of correcting the spectra indicated here assumed that inlet flow distortion had a negligible effect on the broadband noise generated by the fan. The fact that the front quadrant broadband levels of the three configurations shown in figure 7(a) were very similar above about 3000 hertz substantiates that this was a valid assumption. The aft quadrant broadband levels in the rear-drive version were greatly influenced by the additional noise due to the exhaust flow. Thus it was not possible to determine if there was any effect of distortion on broadband noise in the aft quadrant.

Rating techniques. - As a baseline comparison, the measured spectra were used to compute sideline perceived noise levels, PNdB (ref. 6). Sideline distances of 305 meters (1000 ft) and 113 meters (370 ft) were chosen as representative of the altitude of an airplane at the FAA noise certification points for takeoff and approach, respectively. In figure 11 PNdB comparisons are shown for both front-drive installations. Excepting the previously discussed questionable readings at nominal angles of 20° and 50° , the levels are generally the same for the two installations.

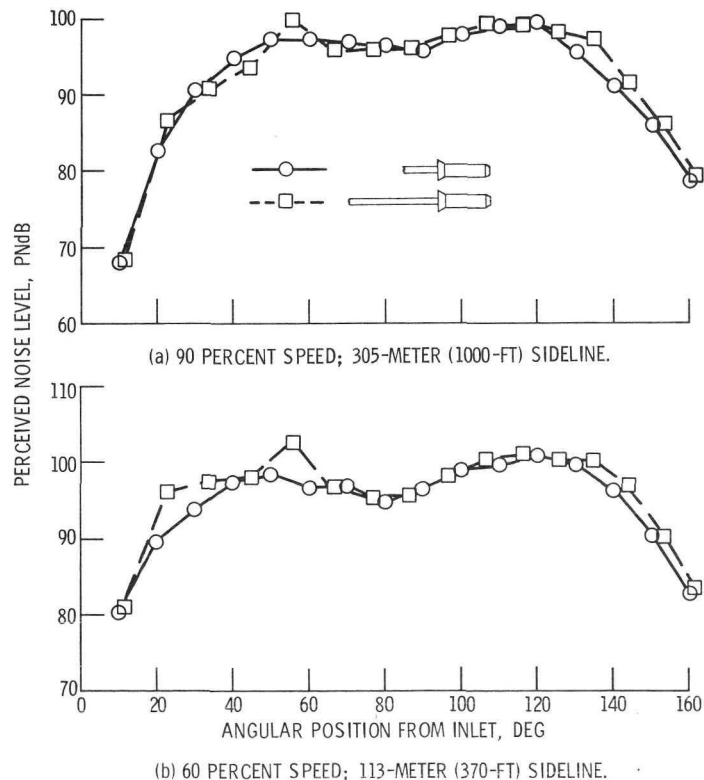


Figure 11. - Comparison of sideline perceived noise level for long- and short-shaft front-drive configurations.

Correcting the one-third octave spectra as described in the previous section and recomputing the PNdB resulted in the comparisons shown in figures 12 and 13. At 90 percent speed (fig. 12) significant differences, as much as 6 PNdB, were noted in the front quadrant. As expected from the blade-passage tone comparisons (fig. 8) smaller differences resulted in the aft quadrant. At 60 percent speed (fig. 13) the corrections for discrete tones resulted in only 2 PNdB or less over almost the entire angular range.

One important rating for a fan or engine is its maximum sideline PNdB. Since the fans tested in this study had their maximum PNdB level occur in the aft quadrant (neglecting the nominal 50° measurement) where the blade-passage tone was less affected by flow distortion than front quadrant blade passage tone, the maximum PNdB rating was only affected by 2 PNdB or less. However, if a fan were tested whose maximum level occurred in the front quadrant and if this level were considerably higher than the aft quadrant levels, significantly higher maximum PNdB levels than for a clean inlet could result.

Another more comprehensive rating technique is the effective perceived noise level (EPNL) computed from a one-third octave spectrum as described in reference 7. The calculation technique accounts for both the level and duration of the sound heard by an

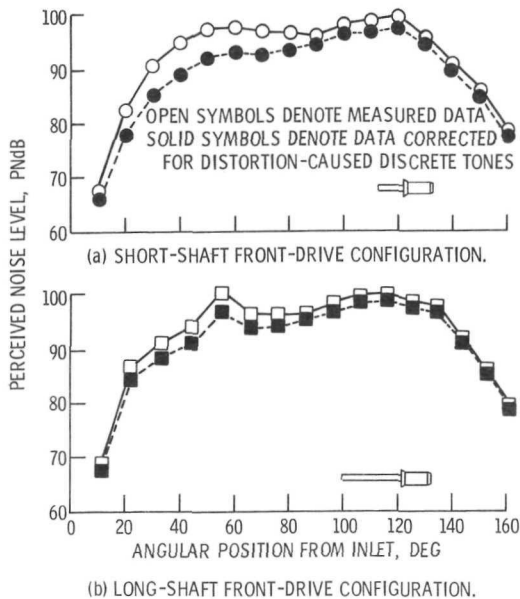


Figure 12. - Comparison of measured sideline perceived noise levels with perceived noise levels corrected for distortion-caused discrete tones; 90 percent speed; 305-meter (1000-ft) sideline.

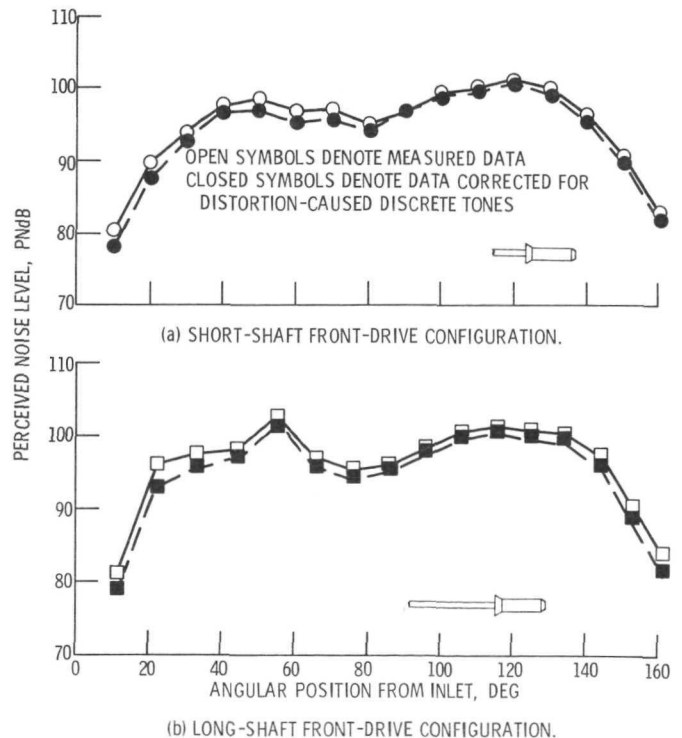


Figure 13. - Comparison of measured sideline perceived noise levels with perceived noise levels corrected for distortion-caused discrete tones; 60 percent speed; 113-meter (370-ft) sideline.

OPEN SYMBOLS DENOTE MEASURED DATA
 CLOSED SYMBOLS DENOTE DATA CORRECTED FOR DISTORTION-
 CAUSED DISCRETE TONES

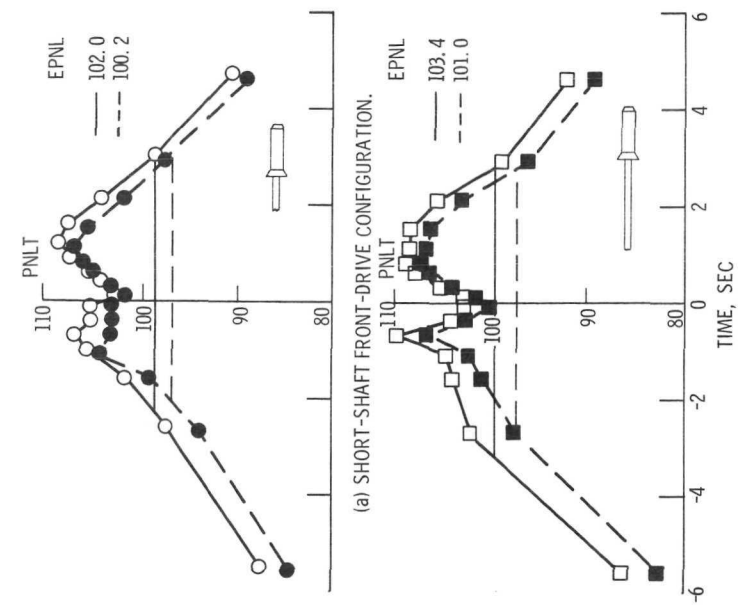


Figure 15. - Comparison of tone-corrected perceived noise levels (PNLT) and effective perceived noise levels (EPNL) for measured data and data corrected for distortion-caused discrete tones; 60 percent speed, 113-meter (370-ft) separation distance; 85.1-meter-per-second (279-ft/sec) flight velocity; four fans.

OPEN SYMBOLS DENOTE MEASURED DATA
 CLOSED SYMBOLS DENOTE DATA CORRECTED FOR DISTORTION-CAUSED DISCRETE TONES

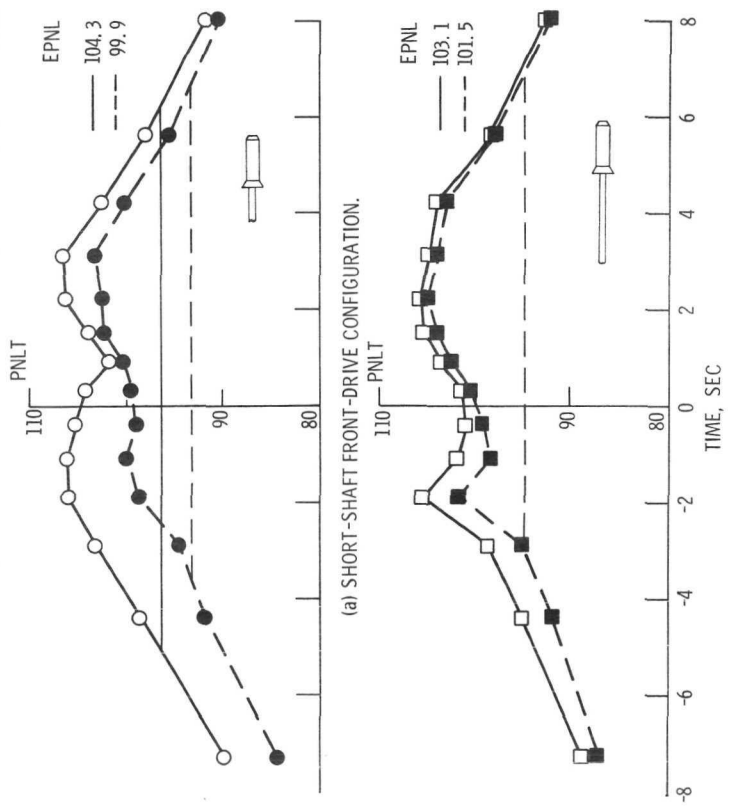




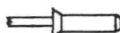
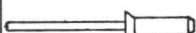


Figure 14. - Comparison of tone-corrected perceived noise levels (PNLT) and effective perceived noise levels (EPNL) for measured data and data corrected for distortion-caused discrete tones; 90 percent speed; 305-meter (1000-ft) separation distance; 85.1-meter-per-second (279-ft/sec) flight velocity; four fans.

observer on the ground as an aircraft flies overhead. The procedure computes tone-corrected perceived noise levels (PNLT) which penalize the spikes in the one-third octave spectrum. These PNL T values, shown in figures 14 and 15 as a function of time, were averaged over the regions bounded by the curves and the 10 dB down lines to derive average PNL T values. A duration correction was then added to the average PNL T to obtain EPNL values.

Figure 14 represents this EPNL calculation at takeoff conditions for the front-drive data as measured and as corrected for discrete tones. A four-fan CTOL aircraft at takeoff speed was simulated at 90 percent speed, at a level flyover height of 305 meters (1000 ft) and at a flight velocity of 85.1 meters per second (279 ft/sec). Figure 15 represents approach conditions. Correcting the data for excessive discrete tone noise caused by inlet flow distortion lowered the EPNL a maximum of 4.4 dB at takeoff for the short-shaft installation, and a maximum of 2.4 dB at approach for the long-shaft installation.

Summary of rating techniques. - Table II lists the dB levels and reductions due to discrete tone corrections of three fan-rating techniques for the two front-drive installations. Data at the nominal 50° angle for the long-shaft installation have been ignored for the maximum PNdB and maximum PNL T sideline comparisons. Takeoff and approach conditions are given. In all cases, correcting the data to the clean inlet discrete tone level, lowered the rating dB level. At takeoff conditions maximum sideline PNdB was reduced 2.1 dB, maximum PNL T for four fans was reduced 3.2 dB, and EPNL was re-

TABLE II. - SUMMARY OF DISCRETE TONE-CORRECTION EFFECTS ON PERCEIVED NOISE LEVEL RATINGS

Noise levels	Installation	Takeoff conditions			Approach conditions		
		Measured data	Data corrected for discrete tones	dB reduction	Measured data	Data corrected for discrete tones	dB reduction
Maximum PNdB on sideline (one fan)		99.4	97.3	2.1	100.9	100.5	0.4
		99.4	98.3	1.1	101.1	100.6	0.5
Maximum PNL T on sideline (four fans)		106.5	103.3	3.2	108.4	106.8	1.6
		105.8	105.0	0.8	108.9	106.8	2.1
EPNdB flyover (four fans)		104.3	99.9	4.4	102.0	100.2	1.8
		103.1	101.5	1.6	103.4	101.0	2.4

duced 4.4 dB. The smaller effects of corrections on the long-shaft version at takeoff were due, in part, to lower discrete tone levels for this installation and also to subtle differences in the heavily weighted one-third octave bands affecting the perceived noise levels. Generally the levels shown in table II were lower and affected more by corrections at takeoff speed than at approach speed.

Distortion Results

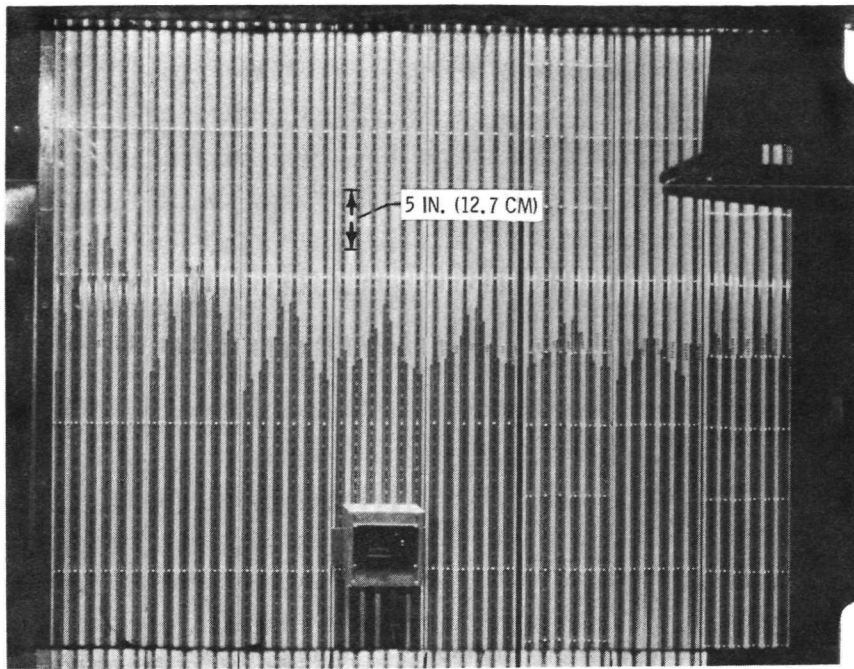
Some previous flow distortion measurements reported in reference 1 showed that a small pressure deficient region existed in the bottom center of the inlet for the short-shaft front-drive installation. The rake used for these measurements had widely spaced pressure tubes and covered approximately a 90° sector. Based on Morse and Ingard's theory (ref. 4) it was postulated that this measured nonuniformity in inlet flow could significantly affect the amplitude of the blade-passage tone. Some observations on a one-sixth scale model of the fan and installation had qualitatively confirmed the distortions measured on the full-scale installation. However, the model tests were not designed to quantify the distortion. Here, in an attempt to better define the origin, extent, and magnitude of the flow distortion in a front-drive installation, some tests were made using the QF-3 fan in the long-shaft front-drive installation.

Total pressure rake. - Inlet total pressures were measured for fan operation at 60 and 90 percent speed using the rake described in the APPARATUS AND PROCEDURE section. The rake was located so as to completely cover the pressure deficient region identified with the rake used in reference 1. One frame of the motion picture film, which was used to record the pressures displayed on the manometer board, is shown in figure 16 for 90 percent fan speed. Each of the first seven 12-tube manometer boards represents one row of pressure tubes in the rake; board number one was attached to the row of tubes closest to the outer wall. The first tube on each board was open to atmosphere. The eighth board was hooked up to miscellaneous tubes from each row.

The movie frame shown in figure 16 represents one of the largest distortions measured. All rows of tubes were affected by the distortion. The greatest pressure defect observed in figure 16 was near the center of each board and thus near the center of the rake. Successive frames show that the distortion fluctuated in amplitude and shifted somewhat in circumferential location but generally was contained within the measuring rake.

The pressure readings from the inlet rake were averaged, converted to velocity, and used for the distortion values in the free propeller theory of Morse and Ingard (ref. 4). Appendix A gives the details of the theory and the assumptions made in applying this propeller theory to the ducted fan used in this study. Comparison of the predicted noise and measured noise is presented in figure 17 where front quadrant sound-

INCHES (CM) OF WATER



BOARD NUMBER 1 2 3 4 5 6 7 MISCELLANEOUS AND SURVEY ROW

Figure 16. - Photograph of inlet rake total pressure readings displayed on manometer board. Fan operating at 90 percent speed.

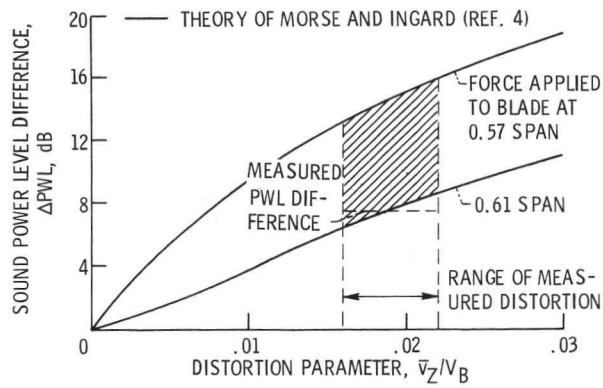


Figure 17. - Sound power level difference for front 90° , 90 percent speed.

power-level difference is shown as a function of a distortion parameter for fan operation at 90 percent speed. The predicted power-level difference is taken between the fan operating with distorted inflow and the fan operating with uniform inflow. Power levels were computed for the blade-passage tone. The velocity ratio is a measure of the distortion; specifically it is the average decrement in axial velocity \bar{v}_Z divided by the blade rotational velocity V_B at the radius where the average distortion acts. Power level differences were calculated for a range of velocity ratios for two values of the mean blade radius at which the mean blade forces are applied. Mean blade radius a_m is determined by adding the hub radius to the percent of span at which the force acts. From detailed blade element data taken on a one-fourth scale model of the QF-1 fan, the mean torque was found to be applied at 57 percent of blade span and the mean thrust force at 61 percent of blade span.

Because of the unsteady nature of the flow distortion, a range of distortion parameter values \bar{v}_Z/V_B representative of the measured pressure fluctuations is shown as the vertical dashed lines in figure 17. The measured sound-power-level difference shown as the horizontal line was obtained from the pressure levels given in figure 8 for the rear-drive installation and the long-shaft front-drive installation. Thus Morse and Ingard's theory for propellers (ref. 4) using measured distortions as inputs, predicted noise level differences comparable to that measured and appears to be a usable theory to predict distortion effects on fan generated noise. Further comments on the applicability of this theory to ducted fans are discussed in appendix A.

Tufts. - In an attempt to locate the origin of the localized inlet flow distortion and to obtain a better idea of the flow field into the inlet, tufts were strung in the vicinity of the inlet as described in the section APPARATUS AND PROCEDURE. Motion pictures of the tuft action during fan operation indicated several possible sources of inlet flow distortion. At the base of the streamlined strut (shown clearly in fig. 18) turbulent tuft action indicated flow separation occurring over the concrete structure. In view of the cluttered unstreamlined nature of this area and its close proximity to the inlet, it is likely that it is a major contributor to the distortion experienced by the fan.

Tuft action in the open area between the two concrete structures was smooth and directed upward and inward toward the inlet. Because of this smooth tuft action, it was concluded that a ground vortex was not a major contributor to the flow distortion in this configuration.

Tufts located underneath and behind the inlet in the vicinity of the two support struts shown in figure 18 showed considerable turbulent flow directed forward into the inlet. Tufts located around the outer fan casing at the bellmouth-inlet flange also showed flow directed toward the inlet. These results indicated that flow was being pulled forward from underneath the inlet. The turbulence indicated that separation was occurring because of the structure in that area. It is felt that proper streamlining of these two regions, one in front of and one underneath and behind the inlet, would greatly improve the



Figure 18. - Closeup view of structures believed to cause inlet flow distortion.

flow into the inlet. This should reduce the front quadrant discrete tones generated by fans tested in the long-shaft front-drive installation.

SUMMARY OF RESULTS

Three installations of essentially the same fan were used to measure fan noise production. In two of the installations the fan was driven by a shaft in the inlet; in the other installation the fan was driven from the rear. The two front-drive configurations were assumed to have more inlet flow distortion than the rear-drive case due to structures in the flow path upstream of the inlet. Differences in fan generated blade-passage tone sound pressure levels of more than 10 dB were observed between the rear-drive and front-drive versions, with the rear-drive installation producing less blade-passage noise. Differences in blade-passage tone were greatest in the front quadrant.

In spite of its greatly reduced blade-passage tone, the rear-drive installation was unacceptable from a noise standpoint because of additional noise generated by exhaust flow over supporting structures.

Noise spectra of the front-drive installations were corrected to have discrete tones of the magnitude measured for the cleaner-inlet, rear-drive configuration. Maximum sideline perceived noise levels were reduced 2 dB or less, maximum tone-corrected

perceived noise levels 3 dB or less, and effective perceived noise levels 4.5 dB or less. In general, these perceived noise levels were lower and affected more at takeoff speed than at approach speed. Thus the NASA Lewis outdoor fan rig in its front-drive configuration provides noise results that are conservative; that is, noisier than would be obtained with a clean inlet flow.

Some inlet distortion data were obtained for a fan in a front-drive installation. Inlet pressure measurements were used in a blade-passage noise production theory to predict the effects of distortion on noise. Good agreement was obtained between the predicted effect and the noise difference measured in the front-drive and rear-drive installations. Tuft tests in the region of the inlet indicated possible origins of the flow distortion.

Lewis Research Center,
National Aeronautics and Space Administration,
Cleveland, Ohio, September 7, 1972,
501-24.

APPENDIX A

PREDICTION OF DISTORTION EFFECTS ON NOISE GENERATION

In reference 4, Morse and Ingard presented an analysis for the sound radiated from a propeller. This analysis follows closely that first developed by Gutin (ref. 8) but also includes the sound radiated when the incoming flow is nonuniform. As a first approximation this theory (ref. 4) has been used to predict the sound radiated from the ducted fan studied herein. Duct effects have not been included here in an attempt to present a simplified calculation and because of the uncertainty of the cutoff theory of Tyler and Sofrin (ref. 9) applying completely under the test conditions of these studies. Although laboratory tests have confirmed cutoff theory, outdoor fan-stage test results given in reference 10 show that cutoff apparently accounts for only a 3- to 5-dB noise reduction as opposed to much larger predicted reductions. This indicates that cutoff may not fully apply except under ideal laboratory conditions where free stream turbulence, for instance, has been held to a minimum.

For the front-drive installations, noise from the type of inlet flow distortion present in the fan inlet would be predicted to propagate because of the modes generated by the interaction of the single cell of distortion and the rotor blades. (The distortion acts as one inlet guide vane in front of the rotor.) These modes would not be cut off but rather would propagate out the inlet as noise. In the rear-drive installation the data show that some blade-passage frequency noise is still present even though cutoff is predicted for this uniform flow configuration. This can be explained if some small amount of singular cell flow distortion still exists caused by the unstreamlined structure underneath and downstream of the inlet. This would not result in a cutoff condition. Or again it is also possible that the cutoff theory does not fully apply in this full-scale outdoor fan test.

Further work may indeed show that consideration of the duct could improve the agreement between prediction and measurement already obtained in this report. Since it is also recognized that the directivity of the sound is probably affected by the presence of the duct, only power levels in the front quadrant were compared between the long-shaft front-drive and rear-drive installations.

The theoretical sound-power-level differences (distortion-case blade-passage tone minus no-distortion-case blade-passage tone) were obtained by using the sound pressures given by equation (A1). This formula is taken from Morse and Ingard (ref. 4, Eq. (11.3.20)) and calculates the sound pressure generated by a propeller at the blade-passage frequency and its harmonics. The formula is the following with some slight changes in nomenclature (Symbols are defined in appendix B):

$$\begin{aligned}
p = \frac{1}{2\pi r} \sum_{N=1}^{\infty} NK_1 \alpha_N \left\{ \sum_{l=0}^{\infty} \left(\delta_l \frac{NB-l}{NBM} F_d - \beta_l F_t \cos \theta \right) \right. \\
\times J_{NB-l}(NBM \sin \theta) \times \sin \left[NK_1(r-ct) + (NB-l) \left(\varphi + \frac{\pi}{2} \right) \right] \\
+ \sum_{l=0}^{\infty} \left(\delta_l \frac{NB+l}{NBM} F_d - \beta_l F_t \cos \theta \right) \\
\left. \times J_{NB+l}(NBM \sin \theta) \times \sin \left[NK_1(r-ct) + (NB+l) \left(\varphi + \frac{\pi}{2} \right) \right] \right\} \quad (A1)
\end{aligned}$$

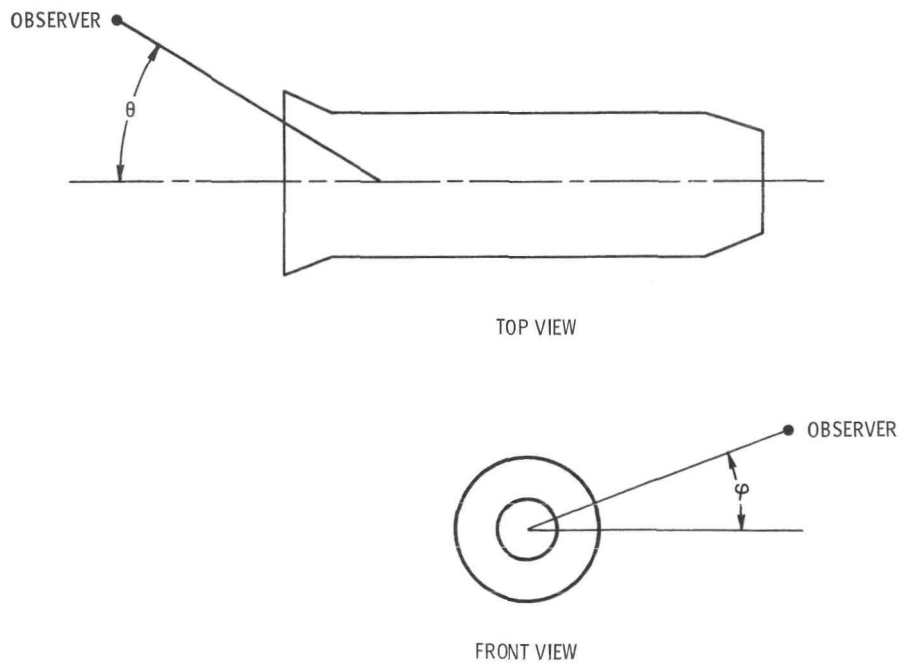


Figure 19. - Definitions of angles used in equation (A1).

The geometry of the situation is shown in figure 19.

As the blade-passage frequency is of interest, the summation over N becomes only one term with $N = 1$. In addition, since the microphones are on the same level as the fan centerline, $\varphi = 0$. The equation then becomes

$$\begin{aligned}
 p = \frac{K_1 \alpha_1}{2\pi r} & \left\{ \sum_{l=0}^{\infty} \left(\delta_l \frac{B-l}{BM} F_d - \beta_l F_t \cos \theta \right) \right. \\
 & \times J_{B-l}(BM \sin \theta) \times \sin \left[K_1(r - ct) + (B-l) \left(\frac{\pi}{2} \right) \right] \\
 & + \sum_{l=0}^{\infty} \left(\delta_l \frac{B+l}{BM} F_d - \beta_l F_t \cos \theta \right) \\
 & \left. \times J_{B+l}(BM \sin \theta) \times \sin \left[K_1(r - ct) + (B+l) \left(\frac{\pi}{2} \right) \right] \right\} \quad (A2)
 \end{aligned}$$

The following outlines the quantities used to evaluate equation (A2). The QF-2 fan has 53 rotor blades and at 90 percent speed turns at approximately 3197 rpm. So,

$$K_1 = \frac{\omega_1}{c} = \frac{B\Omega}{c} = 8.233 \text{ 1/meter (2.53 1/ft)}$$

and

$$r = 30.5 \text{ meters (100 ft)}$$

Also, α_1 is the Fourier coefficient for the first mode (blade-passage frequency) of the blade force Fourier analysis in the rotational direction. This is evaluated using the same assumptions as are expressed in Morse and Ingard (p. 740), which gives

$$\alpha_1 = \frac{\sin \frac{b\pi}{d}}{2\left(\frac{b\pi}{d}\right)} \quad (\text{A3})$$

For purposes of calculation, b/d was taken as $1/2$ giving $\alpha_1 = 1/\pi$. For $0 < b/d < 1$, the calculated power level differences are identical.

The evaluation of β_l and δ_l is a little more complicated, however. Morse and Ingard (on p. 741) discuss the evaluation of β_l and δ_l . This evaluation is done by assuming an airfoil with a constant linear lift curve slope and determining the change in lift and drag forces resulting from an incoming velocity defect. This lift curve slope is assumed not to be influenced by the frequency at which the velocity defect is seen by the blade. This analysis gives, for a velocity defect v_Z in the axial direction,

$$1 + \frac{1}{c_t} \frac{dc_t}{d\tau} \frac{v_Z(\varphi_1)}{V_B} = \sum_l \beta_l e^{il\varphi_1} \quad (\text{A4})$$

and

$$1 + \frac{1}{c_d} \frac{dc_d}{d\tau} \frac{v_Z(\varphi_1)}{V_B} = \sum_l \delta_l e^{il\varphi_1} \quad (\text{A5})$$

The velocity defect v_Z is a function of the angle around the fan disc φ_1 . In this case, the distortion is only over a small part of the fan disc (fig. 20). In order to simplify the calculations, an average velocity defect \bar{v}_Z is taken as occurring over the angular region $-T$ to $+T$.

When this is Fourier analyzed, the coefficients become

$$\beta_0 = 1 + \frac{1}{\pi c_t} \frac{dc_t}{d\tau} \frac{\bar{v}_Z}{V_B} T \quad (\text{A6})$$

$$\beta_l = \frac{1}{l\pi c_t} \frac{dc_t}{d\tau} \frac{\bar{v}_Z}{V_B} \sin(lT) \quad \text{for } l > 0 \quad (\text{A7})$$

and

$$\delta_0 = 1 + \frac{1}{\pi c_d} \frac{dc_d}{d\tau} \frac{\bar{v}_Z}{V_B} T \quad (A8)$$

$$\delta_l = \frac{1}{l \pi c_d} \frac{dc_d}{d\tau} \frac{\bar{v}_Z}{V_B} \sin(lT) \quad \text{for } l > 0 \quad (A9)$$

The analysis of Morse and Ingard assumes that these coefficients are applied from inner to outer radius (the sector-shaped area in fig. 20). However, the distortion only

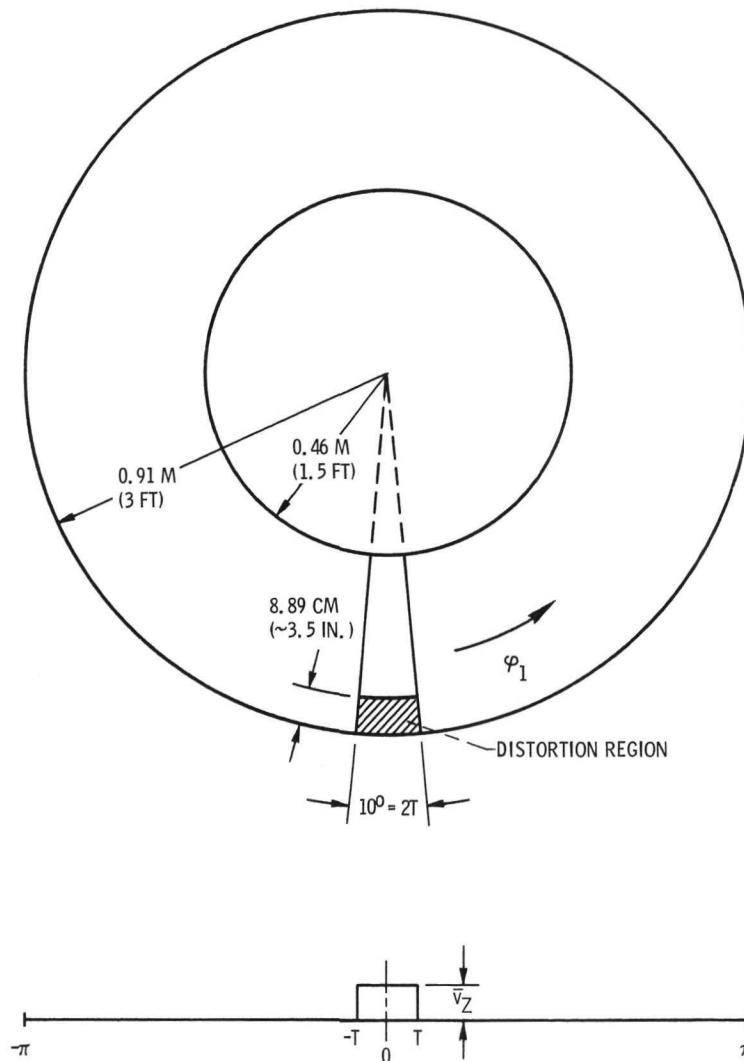


Figure 20. - Extent and characterization of distortion.

occurs over a fraction of the radial dimension, out near the tip. For this reason, it is necessary to also factor in this area ratio effect.

The evaluation of the sound pressure (eq. (A2)) is then handled as follows. First, the summations are broken up into two parts, the $l = 0$ terms and all the remaining terms in the summation. Then the $l = 0$ part is further broken up into that part which is the no-distortion part of the $l = 0$ term and that part which comes from the distortion. The part of the $l = 0$ term that comes from the distortion and all the terms for $l > 0$ (which also arise from the distortion) are then multiplied by the constant A_R , where A_R is the ratio of the area in the distortion region to the area in the large sector-shaped region. The equation divided into these three parts is

$$\begin{aligned}
 p = & \frac{K_1 \alpha_1}{2\pi r} \left\{ \underbrace{\left[2 \left(\frac{F_d}{M_{ND}} - F_t \cos \theta \right) J_B(BM_{ND} \sin \theta) \sin \left[K_1(r - ct) + \frac{B\pi}{2} \right] \right]}_{(l = 0 \text{ no-distortion part})} \right. \\
 & + A_R \underbrace{\left[2 \left(\frac{1}{\pi c_d} \frac{dc_d}{d\tau} \frac{\bar{v}_Z}{V_B} T F_d - \frac{1}{\pi c_t} \frac{dc_t}{d\tau} \frac{\bar{v}_Z}{V_B} T F_t \cos \theta \right) J_B(BM_D \sin \theta) \sin \left[K_1(r - ct) + \frac{B\pi}{2} \right] \right]}_{(l = 0 \text{ distortion part})} \\
 & + A_R \underbrace{\left[\sum_{l=1}^{\infty} \left(\frac{F_d(B-l)}{BM_D^l \pi c_d} \frac{dc_d}{d\tau} \frac{\bar{v}_Z}{V_B} \sin(lT) - \frac{F_t \cos \theta}{l \pi c_t} \frac{dc_t}{d\tau} \frac{\bar{v}_Z}{V_B} \sin(lT) \right) J_{B-l}(BM_D \sin \theta) \sin \left[K_1(r - ct) + (B-l) \frac{\pi}{2} \right] \right]}_{(l > 0 \text{ distortion terms})} \\
 & + \underbrace{\left[\sum_{l=1}^{\infty} \left(\frac{F_d(B+l)}{BM_D^l \pi c_d} \frac{dc_d}{d\tau} \frac{\bar{v}_Z}{V_B} \sin(lT) - \frac{F_t \cos \theta}{l \pi c_t} \frac{dc_t}{d\tau} \frac{\bar{v}_Z}{V_B} \sin(lT) \right) J_{B+l}(BM_D \sin \theta) \sin \left[K_1(r - ct) + (B+l) \frac{\pi}{2} \right] \right]}_{(l > 0 \text{ distortion terms})} \left. \right\} \quad (A10)
 \end{aligned}$$

It should be noted here that the no-distortion part and the distortion part have different rotational Mach numbers (M_{ND} and M_D). This is done because the mean radius for the force application is different in the two cases. This point will be discussed later.

In evaluating the β_l 's and δ_l 's, the following values were used:

$$c_t = 0.49$$

$$c_d = 0.47$$

$$\frac{dc_t}{d\tau} = \frac{dc_d}{d\tau} = 0.628$$

These values were calculated from aerodynamic blade element data measured in a one-fourth scale model of QF-1.

The pressures measured by the distortion rake indicated that the velocity defect almost entirely covered the width of the rake. This gave a distortion approximately 10° wide. The value of T is then about 5° or 0.0875 radian. The radial distance of the distortion extended about 8.9 centimeters ($3\frac{1}{2}$ in.) in from the outside wall. This gave an area ratio A_R of 0.25.

The maximum distortion measured by the distortion rake, when averaged over the area of the rake, gave a distortion parameter \bar{v}_Z/V_B of 0.022. Since this distortion was moving in and out of the small rake (i.e., shifting in circumferential location), a number of averages of the distortion were taken at different times when the distortion was in the rake. The minimum of these averages gave a distortion parameter of approximately 0.016. This value was used for the lower limit on the distortion parameter range. It is felt that the distortion was always present in the inlet and of a magnitude within the limits given but that at times it was not at the same circumferential position as the rake.

As mentioned previously, the no-distortion parts and the distortion parts of the summation have different mean radii for the force application. The distortion terms have a mean radius somewhere inside the distortion area. The center of this distortion area is about 0.9 of the blade span (tip radius minus hub radius). The hub radius plus 0.9 of the span yields a_m for the distortion terms. The mean radius for the no-distortion part is not so well defined. Scale testing on a one-fourth scale model fan has determined that the mean location for the thrust force on this fan is 0.61 and the mean location for the torque is 0.57 of the span. The mean force location is then somewhere between 0.57 and 0.61 of the blade span. These values are then taken as the two limits for calculating a_m ($a_m =$ hub radius plus 0.57 to 0.61 of the blade span). With these radii a_m and the rpm of the fan, the Mach numbers used for the distortion and no-distortion parts are easily calculated. The total force F_t is 90 299 newtons (20 300 lb) and $T = 38\ 098$ joules (28 100 ft-lb) which then allows for the computation of $F_d(F_d = T/a_m)$.

These values were then applied to equation (A10) and the summations taken. The value of the summation varies with time in this equation. This is the variation of sound pressure with time. The rms value of the sound pressure was then calculated for both the no-distortion and the distortion cases at each angle. The sound pressure level in decibels was then calculated at each angle for both cases and the sound power level was calculated for the front 90° . The difference in sound power level, for the front 90° , between the distortion and no-distortion cases was then plotted (see fig. 17).

Figure 17 is a plot of sound power level difference as a function of distortion parameter \bar{v}_Z/V_B . Two curves have been drawn for values of the no-distortion force application location of 0.57 and 0.61 of the blade span. The dashed vertical lines are the values that mark the range for the amount of measured inlet distortion. The dashed horizontal line is the value of the experimentally observed power level difference.

As can be seen, the experimentally observed number partly falls in between the two curves (0.57 to 0.61 span) for the values of the measured distortion. This relatively good agreement points to the value of this method in predicting noise increases from inlet flow distortions.

The measured noise difference is in the lower part of the calculated band, indicating that the calculation method slightly overpredicts the noise increase caused by the inlet flow distortion. A number of reasons exist for this overprediction.

The calculation of the force fluctuation on the rotor blades caused by the inlet flow distortion may be too high. The method used by Morse and Ingard as mentioned before assumed that the lift curve slope is not influenced by the frequency at which the blade experiences the velocity defect. However, it is likely that the blades do not respond instantaneously to a change in angle of attack as shown in references 11 to 13. Thus, the larger magnitude of the force fluctuation used in Morse and Ingard could be resulting in the slight overprediction of this method.

Another possible explanation for the overprediction stems from the fact that the amount of the inlet flow distortion was measured only on the long-shaft front-drive fan installation. No distortion measurements were made on the rear-drive installation. The experimentally measured sound power level differences were made assuming that no distortion existed in the rear-drive configuration. It is possible, however, that some distortion may still exist in the rear-drive case. If this is true, then the experimentally determined sound power level difference may be lower than what would have been obtained if the rear-drive case were completely distortion free.

It is also recognized that in a completely rigorous analysis of distortion effects on ducted fan generated noise, the duct effects should be included. Whether or not the theory of reference 9 should be modified to further account for cutoff in nonideal flow environments will require additional study and more experimental evidence.

Even though a number of simplifying assumptions have been made in the application of the Morse and Ingard theory to the problem at hand, the agreement between prediction and measurement is quite good, and the theory could be applicable as a first approximation of the noise increases from different types and amounts of flow distortion.

APPENDIX B

SYMBOLS

a_m	mean radius on fan disc where forces act (length)
A_R	ratio of area in distortion region to area in sector (fig. 20)
B	number of rotor blades
b	blade width (length)
c	speed of sound (length/time)
c_d	"drag" coefficient (coefficient in tangential direction)
c_t	thrust coefficient
d	distance between blades (length)
$\frac{dc_d}{d\tau}, \frac{dc_t}{d\tau}$	rate of change of drag and thrust coefficients, respectively, with angle of attack
F_d	total drag force, Q/a_m (force)
F_t	total thrust force (force)
$J_x(Y)$	Bessel function of first kind with order X and argument Y
K_1	ω_1/c (1/length)
l	summation index on Fourier analysis of distortion
M	rotational Mach number at mean radius, $a_m \Omega/c$
N	summation index on Fourier analysis of harmonic order (blade-passage frequency has $N = 1$)
p	sound pressure (force/length ²)
Q	total torque (force \times length)
r	radius of observer from center of fan face (length)
T	one-half of angular extent of distortion, radians
t	time
V_B	blade velocity in circumferential direction at mean location of distortion (length/time)
\bar{v}_Z	velocity defect in axial direction (length/time)

α_N	Fourier coefficient in analysis of force on blade for uniform flow (no distortion)
β_l, δ_l	Fourier coefficient of distortion force analysis. (For no distortion: $\beta_0 = \delta_0 = 1$ and $\beta_l = \delta_l = 1$ when $l > 0$)
θ	angle measured from inlet to exhaust around fan, radians (inlet = 0, exhaust = π (fig. 19))
τ	angle of attack, radians
φ	angle above center plane of fan, radians (If observer is on same plane as fan, $\varphi = 0$ (fig. 19))
φ_1	angle around fan disc (fig. 20), radians
ω_1	blade-passage frequency (1/time)
Ω	angular velocity of fan (1/time)

Subscripts:

D	distortion
ND	no distortion

REFERENCES

1. Leonard, Bruce R.; Schmiedlin, Ralph F.; Stakolich, Edward G.; and Neumann, Harvey E.: Acoustic and Aerodynamic Performance of a 6-Foot-Diameter Fan for Turbofan Engines. I - Design of Facility and QF-1 Fan. NASA TN D-5877, 1970.
2. Goldstein, Arthur W.; Lucas, James G.; and Balombin, Joseph R.: Acoustic and Aerodynamic Performance of a 6-Foot-Diameter Fan for Turbofan Engines. II - Performance of QF-1 Fan in Nacelle Without Acoustic Suppression. NASA TN D-6080, 1970.
3. Rice, Edward J.; Feiler, Charles E.; and Acker, Loren W.: Acoustic and Aerodynamic Performance of a 6-Foot-Diameter Fan for Turbofan Engines. III - Performance With Noise Suppressors. NASA TN D-6178, 1971.
4. Morse, Philip M.; and Ingard, J. Uno: Theoretical Acoustics. McGraw-Hill Book Co., Inc., 1968, pp. 737-750.
5. Anon.: Standard Values of Atmospheric Absorption as a Function of Temperature and Humidity for Use in Evaluating Aircraft Fly-Over Noise. Aerospace Recommended Practice 866, SAE, 1964.
6. Anon.: Definitions and Procedures for Computing the Perceived Noise Level of Aircraft Noise. Aerospace Recommended Procedure 865A, SAE, Aug. 1969.
7. Anon.: Noise Standards: Aircraft Type Certification. Vol. III, Part 36 of Federal Aviation Regulations.
8. Gutin, L.: On the Sound Field of a Rotating Propeller. NACA TM-1195, 1948.
9. Tyler, J. M.; and Sofrin, T. G.: Axial Flow Compressor Noise Studies. Trans. SAE, vol. 70, 1962, pp. 309-332.
10. Kramer, James J.; Hartmann, Melvin J.; Leonard, Bruce R.; Klapproth, Jack F.; and Sofrin, Thomas G.: Fan Noise and Performance. Section II of Aircraft Engine Noise Reduction. NASA SP-311, 1972.
11. Sears, William R.: Some Aspects of Non-Stationary Airfoil Theory and Its Practical Application. J. Aeron. Sci., vol. 8, no. 3, Jan. 1941, pp. 104-108.
12. Kemp, Nelson H.; and Sears, W. R.: The Unsteady Forces Due to Viscous Wakes in Turbomachines. J. Aeron. Sci., vol. 22, no. 7, July 1955, pp. 478-483.
13. Horlock, J. H.: Fluctuating Lift Forces on Aerofoils Moving Through Transverse and Chordwise Gusts. J. Basic. Eng., vol. 90, no. 4, Dec. 1968, pp. 494-500.



POSTMASTER: If Undeliverable (Section 158
Postal Manual) Do Not Return

"The aeronautical and space activities of the United States shall be conducted so as to contribute . . . to the expansion of human knowledge of phenomena in the atmosphere and space. The Administration shall provide for the widest practicable and appropriate dissemination of information concerning its activities and the results thereof."

—NATIONAL AERONAUTICS AND SPACE ACT OF 1958

NASA SCIENTIFIC AND TECHNICAL PUBLICATIONS

TECHNICAL REPORTS: Scientific and technical information considered important, complete, and a lasting contribution to existing knowledge.

TECHNICAL NOTES: Information less broad in scope but nevertheless of importance as a contribution to existing knowledge.

TECHNICAL MEMORANDUMS: Information receiving limited distribution because of preliminary data, security classification, or other reasons. Also includes conference proceedings with either limited or unlimited distribution.

CONTRACTOR REPORTS: Scientific and technical information generated under a NASA contract or grant and considered an important contribution to existing knowledge.

TECHNICAL TRANSLATIONS: Information published in a foreign language considered to merit NASA distribution in English.

SPECIAL PUBLICATIONS: Information derived from or of value to NASA activities. Publications include final reports of major projects, monographs, data compilations, handbooks, sourcebooks, and special bibliographies.

TECHNOLOGY UTILIZATION PUBLICATIONS: Information on technology used by NASA that may be of particular interest in commercial and other non-aerospace applications. Publications include Tech Briefs, Technology Utilization Reports and Technology Surveys.

Details on the availability of these publications may be obtained from:

SCIENTIFIC AND TECHNICAL INFORMATION OFFICE

NATIONAL AERONAUTICS AND SPACE ADMINISTRATION

Washington, D.C. 20546